Active Contour Segmentation based on Approximate Entropy
Application to Cell Membrane Segmentation in Confocal Microscopy

Aymeric Histace[1], Elizabeth Bonnefoye[1], Luis Garrido[2], Bogdan J. Matuszewski[3] and Mark Murphy[4]
[1]*ETIS UMR 8051 CNRS /ENSEA/ Cergy-Pontoise University, 95000 Cergy, France*
[2]*Image Processing Group, Universitat de Barcelona, Barcelona, Spain*
[3]*ADSIP Research Centre, University of Central Lancashire, Preston, U.K.*
[4]*Liverpool John Moores University, Liverpool, U.K.*

Keywords: Image Segmentation, Active Contours, Approximate Entropy, Confocal Microscopy.

Abstract: Segmentation of cellular structures is of primary interest in cell imaging for cell shape reconstruction and to provide crucial information about possible cell morphology changes during radiotherapy for instance. From the particular perspective of predictive oncology, this paper reports on a novel method for membrane segmentation from single channel actin tagged fluorescence confocal microscopy images, which remains a challenging task. Proposed method is based on the use of the Approximate Entropy formerly introduced by Pincus embedded within a Geodesic Active Contour approach. Approximate Entropy can be seen as an estimator of the regularity of a particular sequence of values and, consequently, can be used as an edge detector. In this prospective study, a preliminary study on Approximate Entropy as an edge detector function is first proposed with a particular focus on the robustness to noise, and some promising membrane segmentation results obtained on confocal microscopy images are also shown.

1 INTRODUCTION

Segmentation of cellular structures is an essential tool in cell imaging as it enables measurements which can be used to track cell divisions or help to reconstruct corresponding cell lineage tree providing data for calculation of different parameters like cell proliferation rate for instance.

More specifically, the work presented in this paper has been carried out in a context of analyzing changes of cell cytoskeleton properties in a response to ionizing radiation insult. The final goal of this research effort is to better understand cell bio-mechanical responses during cancer radiation therapy by providing in fine to biologists a Computer-Assisted-Analysis tool of the microscopy images making easier the processing of the large amount of data.

To date, only few methods propose to address segmentation of cell structures in fluorescence confocal microscopy images (FCMI) (Ortiz De Solorzano et al., 1999; Sarti et al., 2002; Yan et al., 2008; Mosaliganti et al., 2009; Zanella et al., 2010; Pop, 2011; Meziou et al., 2011; Meziou et al., 2012), and if nuclei can be considered as a feasible task, membrane segmentation remains a real challenge because of the difficulty to find a biological marker making possible a satisfying emphasis of a constituting protein.

In (Matuszewski et al., 2011), and (Histace et al., 2013), it is shown that single actin-tagged acquisitions are of real interest for automatic segmentation of the complete cell cytoskeleton (nuclei, membrane, cytoplasm) using a single biologic marker: most precisely, a complete scheme for nuclei segmentation based on level-set active contour using a fractional entropy descriptor is proposed.

However, because of the strong acquisition noise and the lack of homogeneity of the biological marker when diffusing, the cell membrane segmentation on that particular type of images remains a real challenge mostly because of the difficulty to extract reliable boundary information.

We propose in this paper a prospective study focusing on this particular task. Most precisely, we introduce "Approximate Entropy" as a possible robust edge detector and embed it into a Geodesic Active Contour (GAC) framework for application to segmentation.

The remainder of this paper is organized as follows: in Section 2, the data used in the experiment are described; in Section 3, the segmentation method

Histace A., Bonnefoye E., Garrido L., Matuszewski B. and Murphy M..
Active Contour Segmentation based on Approximate Entropy - Application to Cell Membrane Segmentation in Confocal Microscopy.
DOI: 10.5220/0004903002700277
In *Proceedings of the International Conference on Bio-inspired Systems and Signal Processing* (BIOSIGNALS-2014), pages 270-277
ISBN: 978-989-758-011-6

is presented: Approximate entropy is introduced and detailed, and finally embed into a GAC framework for application to segmentation; Section 4 focuses on experiments on synthetic images and then on the segmentation of cell membrane in confocal microscopy images. Conclusion and Perspective are given in Section 5.

2 FLUORESCENCE CONFOCAL MICROSCOPY IMAGES

The data used in this paper were obtained from human prostate cells (PNT2) which were grown to confluence on glass coverlsips at 37 °C/5% CO_2 in modified Eagles Medium (MEM) supplemented with 10% bovine calf serum, 1% non-essential amino acids and 1 % L-glutamine solution penicillin (100 IU/mL) and streptomycin (100 μg/mL). Once confluent cells were fixed, actin were labelled with phalloidin-FITC according to the manufacturers instructions (Invitrogen, UK). All imaging was carried out using a Zeiss LSM510 confocal microscope. Fig. 1 shows some images extracted at different slice levels from the 3D microconfocal acquisition of the monolayer PNT2 cell culture. The stack volume is defined on the $512 \times 512 \times 98$ grid of pixels each $0.21\,\mu$m $\times$ $0.21\,\mu$m $\times$ $0.11\,\mu$ in size.

The choice of filament actin (F-actin) marker is motivated by the fact that F-actin is believed to play a vital role in cell structure (Hall, 2009). As Actin is one of the three most existing proteins in human cytoskeleton, studying its changes and properties could help discovering weakness of compromised cytoskeleton. This could be finally associated with cancer evolution. As actin is mostly present in the cytoplasm, we can notice that high intensities in slices of Fig. 1 represent the most important part of actin on cell boundaries which allows us to find rough cell membranes whereas darkest areas represent nuclei.

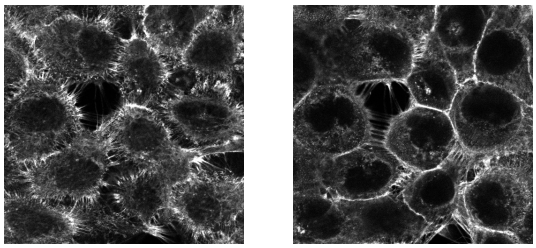

(a) (b)

Figure 1: Examples of actin tagged fluorescence confocal microscopy images extracted from a 3D microconfocal acquisition of the monolayer PNT2 cell culture.

3 THEORY OF SEGMENTATION FRAMEWORK

3.1 Approximate Entropy

Considering gradient-based active contour methods, a real difficulty is still to have an edge detector function with a strong robustness to noise in order to avoid false detection, that leads to non satisfying segmentation (local minimum). Classic gradient operator has limited performance for instance and since 1990 and the former work of Perona and Malik (Perona and Malik, 1990), other boundaries detector have been proposed like the GVF approach. In this article, because of the specificity of the considered images (microconfocal data), we propose to investigate the possibility of using a regularity estimator as a possible edge detector.

Regularity was originally measured by exact regularity statistics, which has mainly centered around various entropy measures (Shanon, Rényi, Tsallis). However, accurate entropy calculation requires vast amounts of data, and the results will be greatly influenced by system noise, therefore it is not practical to apply these methods to experimental data. "Approximate Entropy" ($ApEn$) was developed by Steve M. Pincus in 1991 (Pincus, 1991) to handle these limitations by modifying an exact regularity statistic, Kolmogorov-Sinai entropy. $ApEn$ was initially developed to analyze medical data, such as heart rate (Pincus et al., 1991), and later spread its applications in finance (Pincus and Kalman, 2004), psychology (Pincus and Goldberger, 1994), and human factors engineering (McKinley et al., 2011).

To summarize the mathematical definition of $ApEn$: given an array of size N and an integer m, under the conditions $0 < m \leq N$, a sequence of real numbers $u = (u(1), u(2), ..., u(N))$, and a real number r (where $r \geq 0$), let the distance between two sub-sequences $x(i) = (u(i), u(i+1), ..., u(i+m-1))$ and $x(j) = (u(j), u(j+1), ..., u(j+m-1))$, be defined as $d(x(i), x(j)) = max_{p=1,2,...,m}(|u(i+p-1) - u(j+p-1)|)$. Then let $C_i^m(r) = \{$ number of $j \leq (N-m+1)$ such that $d(x(i), x(j)) \leq r\}/(N-m+1)$. Now define

$$C^m(r) = \frac{1}{N-m+1} \sum_{i=1}^{N-m+1} C_i^m(r) \qquad (1)$$

and finally

$$ApEn(m, r, N) = \ln \left[\frac{C_m(r)}{C_{m+1}(r)} \right] \qquad (2)$$

$ApEn(m,r,N)(u)$ may be interpreted as a measure of the maximum frequency at which number sequences within u of length m occur compared with sequences of length $m+1$. High values of $ApEn$ imply randomness; low values imply order. In (Parker et al., 1999), authors hypothesis that $ApEn$ may be used to distinguish useful image information (edges, textures) from noise. Inspired by the work of Parker et al., this work focuses on the possibility of using $ApEn$ as an edge detector embedded into a GAC framework.

3.2 $ApEn$ in a GAC Framework

GAC were introduced as a geometric alternative for 'snakes'. It is both a geometric model as well as energy functional minimization. Let the curve $\Gamma(p) = \{x(p), y(p)\}$, where $p \in [0,1]$ is an arbitrary parametrization. The GAC model is defined by the energy functional

$$E(\Gamma) = \int_0^1 g\Big[|\nabla I(\Gamma(p))|\Big]|\Gamma'(p)|dp \qquad (3)$$

where $g()$ is a positive edge indicator function that depends on the image I (it gets small values along the edges and higher values elsewhere), and ∇ the gradient operator.

Minimization of Eq. (4) is done using the Euler Lagrange equation as a gradient descent process, and leads to

$$\frac{\partial \Gamma(p,t)}{\partial t} = \Big[g\big(|\nabla I(\Gamma)|\big) - (\nabla g.N)\Big]N \qquad (4)$$

where N is the local normal of the curve Γ.

As said in the introduction of this section, the choice for $g()$ is crucial for the obtaining of satisfying segmentation results. Formerly, Perona-Malik (Perona and Malik, 1990) proposed to define $g()$ as a negative exponential function such that

$$g\big(\nabla I\big) = e^{-\left(\frac{\nabla I}{k}\right)^2} \qquad (5)$$

with k a strictly positive constant to be empirically defined, depending on the application.

What we propose here is to use $ApEn$, instead of the simple gradient operator, for edge detection such as

$$g\big(ApEn(I)\big) = e^{-\left(\frac{ApEn(I)}{k}\right)^2} \qquad (6)$$

Main idea is to be able to cop with strongly noised images like the microconfocal images showed in Section 2.

In the following, $ApEn$ images are computed using a classic square-glindind-window approach of size M such as $M \times M = N$, each line of the $M \times M$ window forming the vector of values used for $ApEn$ computation. With this strategy, there are as many computation of $ApEn$ as the total number of pixels in the image.

4 TESTS AND RESULTS

4.1 Approximate Entropy as an Edge-detector Function

In this section, we focus our attention on the study of $ApEn$ as an efficient edge detector function. For this purpose, we consider the synthetic image showed in Fig. 2 in which a peanut shape is corrupted by zero-mean Gaussian noise of standard-deviation 0.5.

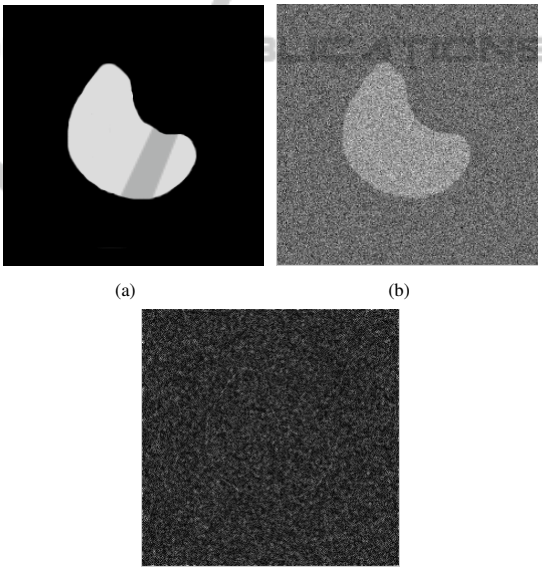

(a) (b)

(c)

Figure 2: (a) Original synthetic image, (b) Image corrupted by a white-Gaussian noise of standard-deviation 0.5, and (c) corresponding gradient image.

For illustration, Fig. 2.(c) shows the corresponding gradient image: it can be noticed, that with such an amount of noise, the edge information is completely lost.

Considering now $ApEn$, first of all influence of parameter r is illustrated. m and M are fixed to arbitrary values, respectively 1 and 9 (following classic values used for application in EEG or ECG data). Fig. 3 shows obtained results for contour detection application. In Fig. 4, for $r = 1.5$, we considered different values for m parameter and finally, Fig. 5 illustrates

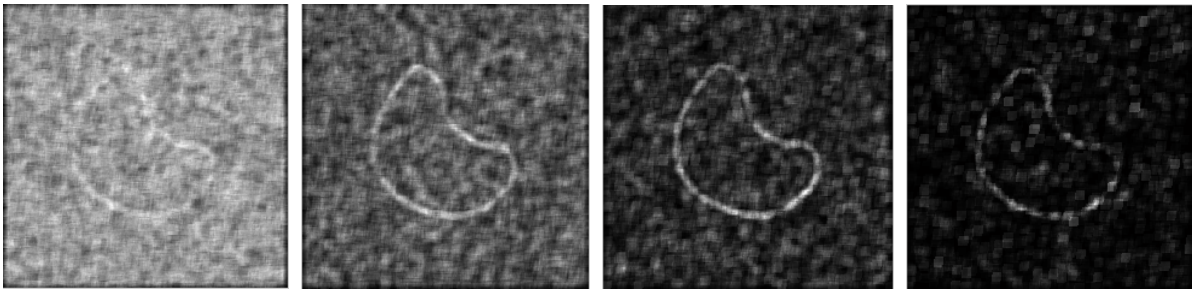

(a) (b) (c) (d)

Figure 3: Different $ApEn$ images for (a) $r = 0.5$, (b) $r = 1$, (c)$r = 1.5$ and finally (d) $r = 2$.

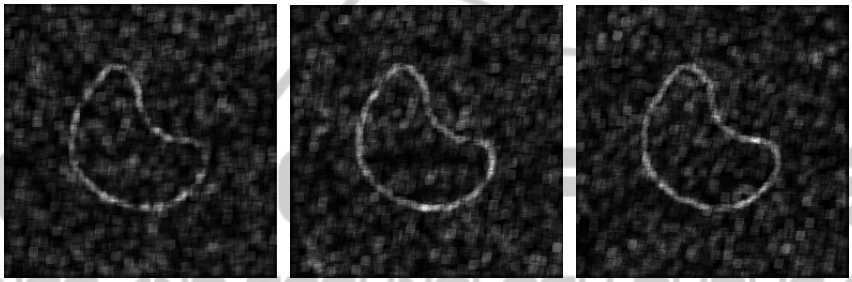

(a) (b) (c)

Figure 4: Different $ApEn$ images for $r = 1.5$ and (a) $m = 1$, (b)$m = 2$, (c) $m = 3$.

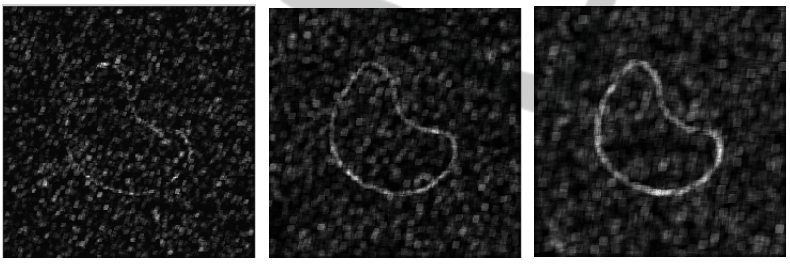

(a) (b) (c)

Figure 5: Different $ApEn$ images for $r = 1.5$, $m = 2$ and (a) $M = 5$, (b) $M = 7$, (c) $M = 9$.

different $ApEn$ images for different values of the size M of the square-window used for $ApEn$ implementation.

First of all, these different figures illustrate that $ApEn$ can be considered as a robust edge detector even in case of a strong corrupting noise. About the influence of the different parameters, r and M are the one with most influence. For a value of r too small, even noise is identified as edge information (see Fig. 3.(a) for instance)) and for a value too important, the threshold value is too selective. For proposed image of Fig. 2, $r = 1.5$ corresponds to the better compromise. Finally parameter m is of less importance, but $m = 2$ allows the obtaining of visually slightly better results.

About parameter M, the size of the square-window used for computation of $ApEn$, if this value has also a strong importance on the edge-detection results, it also strongly influence the computation time because on the kernel-filtering strategy used. Best choice of M should then be based on a compromise between time computation and preciseness of the edge detection. Nevertheless, with $M = 9$, $N = 81$ values of intensity are taken into account for each computation of $ApEn$ computation of $ApEn$, which is statistically more meaningful than with only $N = 25$ values for instance ($M = 5$), or even $N = 49$ ($M = 7$).

4.2 Segmentation Results on Synthetic Images

In this section, we now focus on the efficiency of $ApEn$ when embedded into the GAC framework for segmentation of the noisy peanut shape of Fig. 2.(b). For this purpose, we propose to use the classic level-

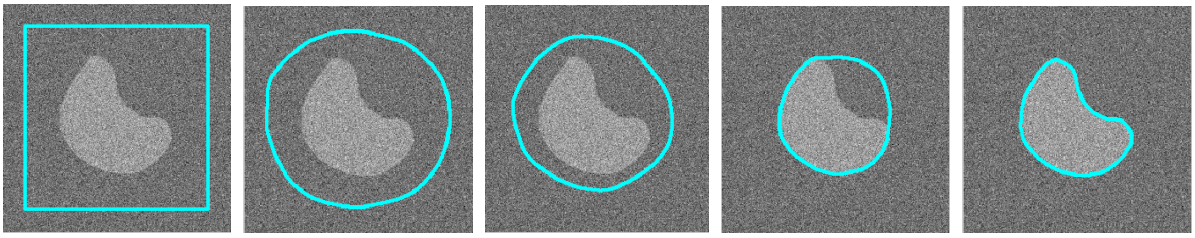

(a) (b) (c) (d) (e)

Figure 6: Segmentation of Fig. 2 using $ApEn$ in a GAC framework. (a) initialization, (b) iteration 100, (c) iteration 200, (d) iteration (300) and (e) final result.

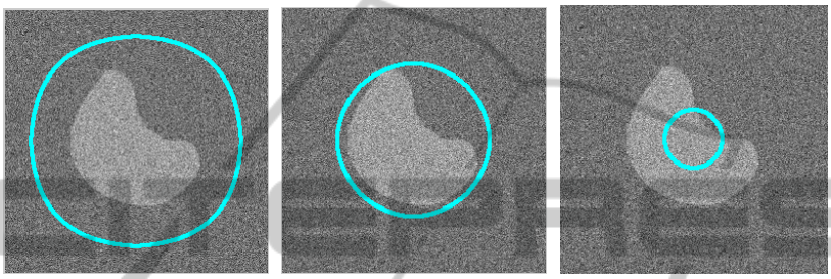

(a) (b) (c)

Figure 7: Segmentation of Fig. 2 using classic gradient operator of GAC framework. (a) iteration 100, (b) iteration 300, (c) iteration (450).

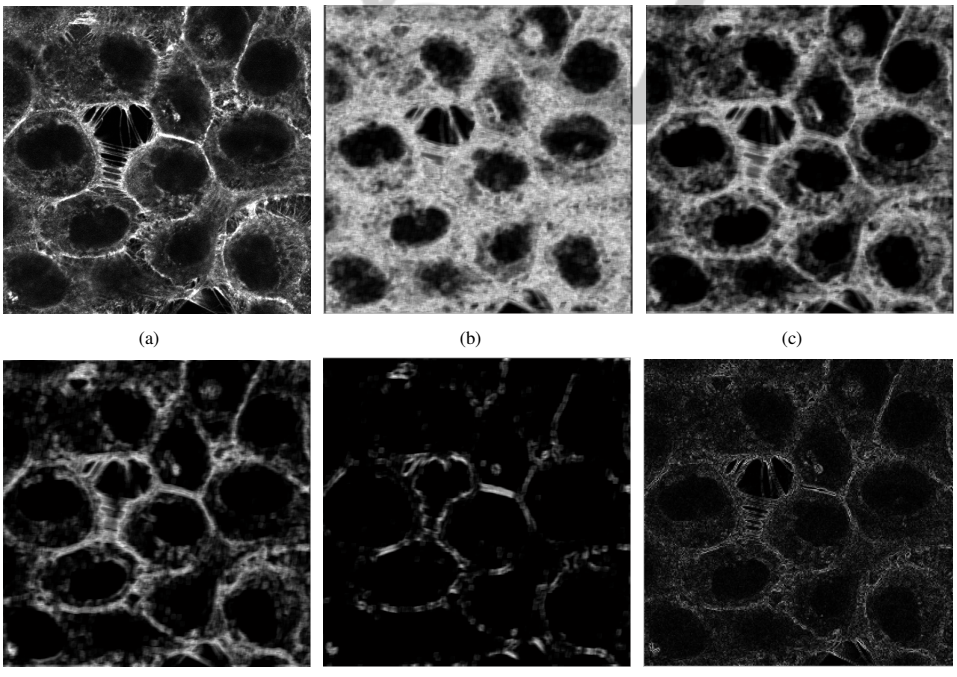

(a) (b) (c)

(d) (e) (f)

Figure 8: $ApEn$ images computed on an actin-tagged microscopy image. For these experiments,$m = 2$, $N = 9$ and different values of r are considered : (b) $r = 0.05$, (c) $r = 0.1$, (d) $r = 0.2$ and (e) $r = 0.5$. Finally (f) is the gradient image obtained on original image.

set approach of (Osher and Sethian, 1988), in a fast implementation configuration (Goldenberg et al., 2001). Initialization of the curve Γ is a squared surrounding the peanut shape. Segmentation result using $ApEn$ parametrized with $r = 1.5$, $m = 2$ and $M = 9$ (i.e. $N = 81$) and Eq. (6) is shown Fig. 6.

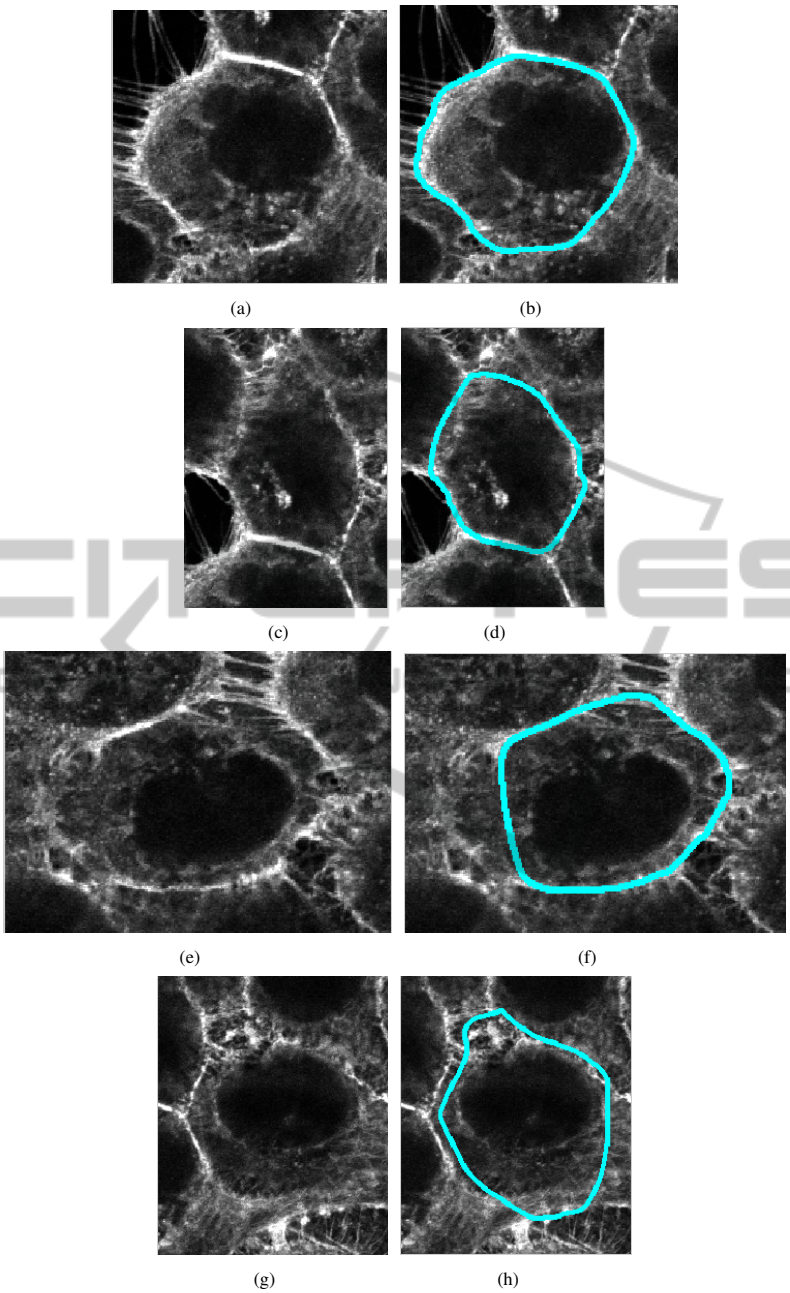

Figure 9: Several examples of membrane segmentation of cell using the *ApEn*-GAC algorithm.

For comparison, segmentation result using Eq. (5) is shown Fig. 7. k parameter was empirically tuned in order to obtain the best visual possible result (here $k = 0.2$) even if the final result shows that segmentation is impossible because of the too strong amount of noise corrupting original image.

These results demonstrate as a proof of feasibility that *ApEn* is of real interest in the framework of active contour segmentation, and most precisely when embedded within a GAC framework. The real ability of *ApEn* to detect edge information, even when images are corrupted with a strong amount of noise, appears here as a significant advantage when compared to classic gradient operator.

4.3 Membrane Segmentation in Confocal Microscopy Images

Coming back to the particular application we focus on, some previous results are presented in this section.

First, Fig. 8 shows $ApEn$ images that were computed for $m = 2$, $M = 9$ (i.e. $N = 81$) and different values of r.

It can be noticed in Fig. 8 that again, it exists a value of r leading to visual interesting results in terms of the emphasis of cell boundaries: more precisely, for $r = 0.2$, a good compromise is obtained between noise removal and emphasis of cell boundaries (membrane). This result, illustrated in Fig. 8.(d), can be compared with Fig. 8.(f) showing the classic gradient image.

About segmentation results using $ApEn$ in GAC framework, we only present here some first results obtained on some crops of an original actin-tagged microscopy image. Initialization strategy is still the same as the previous one, a square-curve surrounding the cell to segment (Fig. 9).

These first results are, from our point of view, quite encouraging when considering the challenging task. Fig. 9 shows that it is possible to properly segment cells even in case where visually the boundary information is not present within the original image (illustrations (d) and (e) for instance). Same Figure also shows some limitations of the proposed criterion that is $ApEn$ when considering subfigure (f). In this case, the size ($M = 9$) of the kernel used for the computation of the $ApEn$ image introduced some uncertainty on the precise location of the cell boundary and lead to an approximative result of segmentation.

5 CONCLUSIONS AND PERSPECTIVE

In this article, we introduced an original approach for image segmentation using GAC framework and Approximate Entropy ($ApEn$) estimation used as an edge detector function. Results are presented on both synthetic and real image, focusing for this latter part on a particular application that is segmentation of cell boundaries in actin-tagged microconfocal images.

As a proof a feasibility, this contribution is a first step towards a better understanding of $ApEn$ for a possible use in image processing and more precisely as a possible criterion for active contour segmentation. Compared to the former work of Parker et al. (Parker et al., 1999) this preliminary study investigates the influence of the different parameters used for computation of $ApEn$ in an image processing context, which was not proposed before.

Main forthcoming perspective will consist in quantitatively estimate the performance of $ApEn$ with respect to the different parameters r, m, and N (via the choice made for the size M of the square-window) in order to possibly go towards an automatic optimization of them (r above all). From the application perspective, if the first results are quite encouraging, we must now proposed a more adapted strategy in terms of initialization in order to be able to segment all the cells in paralell. Moreover, a clinical validation will be also necessary to validate the segmentation process.

REFERENCES

(2011). Image filtering using anisotropic structure tensor for cell membrane enhancement in 3d microscopy. In *Proceedings of International Conference on Image Processing ICIP 2011*, pages 2085–2088.

Goldenberg, R., Kimmel, R., Rivlin, E., and Rudzsky, M. (2001). Fast Geodesic Active Contours. *IEEE TRANSACTIONS ON IMAGE PROCESSING*, 10(10):1467–75.

Hall, A. (2009). *The cytoskeleton and cancer*, volume 28. Springer Netherlands, Philadelphia, PA, USA.

Histace, A., Meziou, L., Matuszewski, B., Precioso, F., Murphy, M., and Carreiras, F. (2013). Statistical region based active contour using a fractional entropy descriptor: Application to nuclei cell segmentation in confocal microscopy images. *Annals of British Machine Vision Association*, 2013(5):1–15.

Matuszewski, B., Murphy, M., Burton, D., Marchant, T., Moore, C., Histace, A., and Precioso, F. (2011). Segmentation of Cellular Structures in Actin Tagged Fluorescence Confocal Microscopy Images. In *IEEE ICIP 2011*, pages pp. 3081–3084, Bruxelles, Belgium.

McKinley, R. A., McIntire, L. K., Schmidt, R., Repperger, D. W., and Caldwell, J. A. (2011). Evaluation of eye metrics as a detector of fatigue. *Human Factors: The Journal of the Human Factors and Ergonomics Society*, 53(4):403–414.

Meziou, L., Histace, A., Precioso, F., Matuszewski, B., and Carreiras, F. (2012). 3D Confocal Microscopy data analysis using level-set segmentation with alpha-divergence similarity measure. In *International Conference on Computer Vision Theory and Applications*, pages 861–864, Rome, Italy.

Meziou, L., Histace, A., Precioso, F., Matuszewski, B., and Murphy, M. (2011). Confocal Microscopy Segmentation Using Active Contour Based on Alpha-Divergence. In *Proceedings of ICIP 2011*, pages 3138–3141.

Mosaliganti, K., Gelas, A., Gouaillard, A., Noche, R., Obholzer, N., and Megason, S. (2009). Detection of spatially correlated objects in 3d images using appearance models and coupled active contours. In *Proceedings of MICCAI'09*, pages 641–648, Berlin, Heidelberg. Springer-Verlag.

Ortiz De Solorzano, C., Garcia Rodriguez, E., Jones, A., Pinkel, D., Gray, J. W., Sudar, D., and Lockett, S. J. (1999). Segmentation of confocal microscope images of cell nuclei in thick tissue sections. *Journal of Microscopy*, 193(3):212–226.

Osher, S. and Sethian, J. A. (1988). Fronts propagating with curvature dependent speed: Algorithms based on hamilton-jacobi formulations. *Journal of Comp. Phy.*, 79:12–49.

Parker, G. J., Schnabel, J. A., and Barker, G. J. (1999). Non-linear smoothing of MR images using approximate entropy – A local measure of signal intensity irregularity. In Kuba, A., Sámal, M., and Todd-Pokropek, A., editors, *Information Processing in Medical Imaging*, volume 1613 of *Lecture Notes in Computer Science*, pages 484–489. Springer Berlin Heidelberg.

Perona, P. and Malik, J. (1990). Scale-space and edge detection using anistropic diffusion. *IEEE Transcations on Pattern Analysis and Machine Intelligence*, 12(7):629–639.

Pincus, S. and Kalman, R. E. (2004). Irregularity, volatility, risk, and financial market time series. *Proceedings of the National Academy of Sciences of the United States of America*, 101(38):13709–13714.

Pincus, S. M. (1991). Approximate entropy as a measure of system complexity. *Proceedings of the National Academy of Sciences*, 88(6):2297–2301.

Pincus, S. M., Gladstone, I. M., and Ehrenkranz, R. A. (1991). A regularity statistic for medical data analysis. *Journal of Clinical Monitoring*, 7(4):335–345.

Pincus, S. M. and Goldberger, A. L. (1994). Physiological time-series analysis: what does regularity quantify? *AJP - Heart and Circulatory Physiology*, 266(4):H1643–1656.

Sarti, A., Malladi, R., and Sethian, J. A. (2002). Subjective surfaces: A geometric model for boundary completion. *Int. J. Comput. Vision*, 46(3):201–221.

Yan, P., Zhou, X., Shah, M., and Wong, S. T. C. (2008). Automatic segmentation of high throughput rnai fluorescent cellular images. *IEEE Transactions on Information Technology in Biomedicine*, 12(1):109–117.

Zanella, C., Campana, M., Rizzi, B., Melani, C., Sanguinetti, G., Bourgine, P., Mikula, K., Peyriéras, N., and Sarti, A. (2010). Cells segmentation from 3d confocal images of early zebrafish embryogenesis. *IEEE trans. on IP*, 19(3):770–781.